AGU PUBLICATIONS

Paleoceanography

RESEARCH ARTICLE
10.1002/2016PA002958

The MMCO-EOT conundrum: Same benthic $\delta^{18}O$, different CO_2

Lennert B. Stap[1], Roderik S. W. van de Wal[1], Bas De Boer[2], Richard Bintanja[3], and Lucas J. Lourens[4]

[1]Institute for Marine and Atmospheric Research Utrecht, Utrecht University, Utrecht, Netherlands, [2]School of Earth and Environment, Faculty of Environment, University of Leeds, Leeds, UK, [3]Royal Netherlands Meteorological Institute (KNMI), De Bilt, Netherlands, [4]Department of Earth Sciences, Faculty of Geosciences, Utrecht University, Utrecht, Netherlands

Key Points:
- Antarctic topographic change explains difference in CO_2 between EOT and MMCO, despite similar $\delta^{18}O$
- This entails a different construction of the $\delta^{18}O$ signal between these episodes
- The result is contingent on how topographic changes are implemented in our ice sheet model

Correspondence to:
L. B. Stap,
L.B.Stap@uu.nl

Citation:
Stap, L. B., R. S. W.van de Wal, B. De Boer, R. Bintanja, and L. J. Lourens (2016), The MMCO-EOT conundrum: Same benthic $\delta^{18}O$, different CO_2, *Paleoceanography*, *31*, 1270–1282, doi:10.1002/2016PA002958.

Received 1 APR 2016
Accepted 29 AUG 2016
Accepted article online 7 SEP 2016
Published online 19 SEP 2016

Abstract Knowledge on climate change during the Cenozoic largely stems from benthic $\delta^{18}O$ records, which document combined effects of deep-sea temperature and ice volume. Information on CO_2 is expanding but remains uncertain and intermittent. Attempts to reconcile $\delta^{18}O$, sea level, and CO_2 by studying proxy data suffer from paucity of data and apparent inconsistencies among different records. One outstanding issue is the difference suggested by proxy CO_2 data between the Eocene-Oligocene boundary (EOT) and the Middle-Miocene Climatic Optimum (MMCO), while similar levels of $\delta^{18}O$ are shown during these times. This conundrum implies changing relations between $\delta^{18}O$, CO_2, and temperature over time. Here we use a coupled climate-ice sheet model, forced by two different benthic $\delta^{18}O$ records, to obtain continuous and mutually consistent records of $\delta^{18}O$, CO_2, temperature, and sea level over the period 38 to 10 Myr ago. We show that the different CO_2 levels between the EOT and MMCO can be explained neither by the standard configuration of our model nor by altering the uncertain ablation parametrization on the East Antarctic Ice Sheet. However, we offer an explanation for the MMCO-EOT conundrum by considering erosion and/or tectonic movement of Antarctica, letting the topography evolve over time. A decreasing height of the Antarctic continent leads to higher surface temperatures, reducing the CO_2 needed to maintain the same ice volume. This also leads to an increasing contribution of ice volume to the $\delta^{18}O$ signal. This result is, however, dependent on how the topographic changes are implemented in our ice sheet model.

1. Introduction

Long-term climate change on Earth is documented by marine benthic $\delta^{18}O$ records [*Lisiecki and Raymo*, 2005; *Zachos et al.*, 2008; *Cramer et al.*, 2009]. They suggest a gradually cooling climate during the Cenozoic, overprinted by more rapid orbital-scale variability and transient excursions. However, the interpretation of the $\delta^{18}O$ signal is complicated by the fact that it comprises contributions from both deep-sea temperature and global ice volume [e.g., *Chappell and Shackleton*, 1986]. To disentangle the $\delta^{18}O$ signal, independent records of either deep-sea temperature [*Lear et al.*, 2000; *Sosdian and Rosenthal*, 2009; *Elderfield et al.*, 2012] or sea level [*Miller et al.*, 2005a; *Kominz et al.*, 2008; *Rohling et al.*, 2014] are required, which are still only scarcely available and possess large uncertainties.

The forcing of the documented climate change is externally determined by variations in solar insolation [*Milankovitch*, 1930]. However, these are not strong enough to explain the amplitude of observed climate variability without any further climate feedbacks [*Imbrie et al.*, 1992]. Furthermore, in contrast to $\delta^{18}O$, the spectral power of solar insolation does not significantly change during the Cenozoic [*Zachos et al.*, 2008; *Laskar et al.*, 2004]. Therefore, insolation variability can neither explain the gradual cooling, nor the excursions documented by benthic $\delta^{18}O$ records. This indicates that internal variability and feedbacks play a crucial role in climate change over time. One factor concerns concentrations of greenhouse gases, such as CO_2, which heat up the atmosphere by trapping long-wave radiation. While a high-fidelity CO_2 record over the past 800 kyr is derived from ice cores [*EPICA community members*, 2006], proxy data records for CO_2 before that time are of low resolution, intermittent, and mutually disagreeing [*Beerling and Royer*, 2011; *Köhler et al.*, 2015]. Attempts to reconcile sea level, temperature, and CO_2 proxy data are hampered by this paucity of data and the mutual inconsistency of data records [*Foster and Rohling*, 2013; *Gasson et al.*, 2012].

An alternative approach to these issues, involving the use of models, is undertaken in this study. Models have the advantage of providing mutually consistent and continuous records. In earlier studies, the benthic

δ^{18}O signal was deconvoluted by using an inverse routine to force a one-dimensional ice sheet model. In this manner, sea level and Northern Hemispheric temperature simulations were obtained over the past 40 Myr [*De Boer et al.*, 2010]. On shorter time scales, this methodology was also applied to a three-dimensional ice sheet model with realistic topography [*Bintanja et al.*, 2005; *Bintanja and Van de Wal*, 2008; *De Boer et al.*, 2013, 2014]. A limitation of these stand-alone ice sheet model studies was that information on climate only consisted of globally uniform perturbations to preindustrial temperatures. Moreover, CO_2 was not explicitly incorporated in the model. Therefore, a hybrid model-data approach was taken by *Van de Wal et al.* [2011] to continuously reconstruct a consistent CO_2 record over the past 20 Myr. They assembled various proxy-CO_2 data records and inferred a log linear relation between Northern Hemispheric temperature and CO_2. In a subsequent study, the one-dimensional ice sheet model was coupled to a zonally averaged energy balance climate model [*Stap et al.*, 2014]. The inverse benthic δ^{18}O routine was modified to simulate CO_2 over the past 5 Myr [*Stap et al.*, 2016], using the stacked benthic δ^{18}O record of *Lisiecki and Raymo* [2005] as input. They simulated benthic δ^{18}O, sea level, temperature, and CO_2 for the first time in a fully coupled fashion over a multimillion year time span.

In this study, we apply this method of deconvoluting δ^{18}O, inversely simulating CO_2 and thereby reconciling these variables, to the period 38 Myr ago to 10 Myr ago. Over this time, we force the same model as *Stap et al.* [2016], explained in section 2, using the stacked benthic δ^{18}O records of *Zachos et al.* [2008] and *Cramer et al.* [2009]. Specifically, we focus on two important warm spells: the time right before the Eocene-Oligocene Transition (EOT; 33.9 Myr ago) and the Middle-Miocene Climatic Optimum (MMCO; 17 to 15 Myr ago). Both these episodes encompass similarly low benthic δ^{18}O values, suggesting comparable warm climates. However, proxy-CO_2 data for right before the EOT [*Pagani et al.*, 2011; *Pearson et al.*, 2009; *Retallack*, 2009] show significantly higher values than for the MMCO [*Pagani et al.*, 1999; *Foster et al.*, 2012; *Greenop et al.*, 2014; *Kürschner et al.*, 2008]. Although earlier modeling studies have addressed the EOT [e.g., *DeConto and Pollard*, 2003; *Pollard and DeConto*, 2005; *Wilson et al.*, 2013; *Ladant et al.*, 2014; *Gasson et al.*, 2014] as well as the MMCO [e.g., *You et al.*, 2009; *Langebroek et al.*, 2009, 2010; *Henrot et al.*, 2010; *Goldner et al.*, 2014], we are the first to transiently simulate a time span covering both events. In doing so, we obtain a consistent representation of the climate during these important times.

We investigate whether we can explain the MMCO-EOT conundrum of similar benthic δ^{18}O but different CO_2, for instance, through a change in the contributions of ice volume and deep-sea temperature to the benthic δ^{18}O signal. In section 3.1, where we use the standard settings of the model and a sensitivity experiment, we do not simulate a difference in CO_2 between right before the EOT and the MMCO. In section 3.2 we analyze simulations with Antarctic topography varying over time, to address the influence of erosion and tectonics. This offers a plausible explanation for the conundrum. However, this result is contingent on the way 3-D topographic changes are transferred to our simplified 1-D model. In section 3.3, we discuss some further factors that can affect the relation between benthic δ^{18}O, which are not incorporated in our setup. Conclusions are presented in section 4.

2. Model and Methods

We use a coupled climate-ice sheet model [*Stap et al.*, 2014], incorporating a routine to calculate benthic δ^{18}O (Figure 1). This model consists of a zonally averaged energy balance climate model [*North*, 1975; *Bintanja*, 1997] coupled to one-dimensional models of the five major Cenozoic ice sheets (Eurasian, North American, Greenland, West Antarctic, and East Antarctic ice sheets) [*De Boer et al.*, 2010]. The climate model has a 5° latitudinal resolution and includes an ocean component with six vertical layers, which simulates the large-scale meridional ocean overturning and contains a 1.25° resolution thermodynamical sea ice routine. The ocean overturning strength varies as a function of the polar to equatorial sea surface temperature difference [*Stap et al.*, 2014]. The calculated local atmospheric surface temperatures are provided to the surface mass balance routine of the ice sheet models. Herein, precipitation (P) follows from present-day precipitation (P_0), corrected for surface air temperature (T), and ice sheet radius (R) with respect to a critical radius (R_c):

$$P = P_0 e^{0.04T - R/R_c}. \quad (1)$$

Accumulation is calculated as a temperature-dependent fraction of precipitation. Ablation M is obtained using an insolation-temperature melt equation [e.g., *Van den Berg et al.*, 2008]:

$$M = [10T + 0.513(1-\alpha)Q + C_{abl}]/100, \quad (2)$$

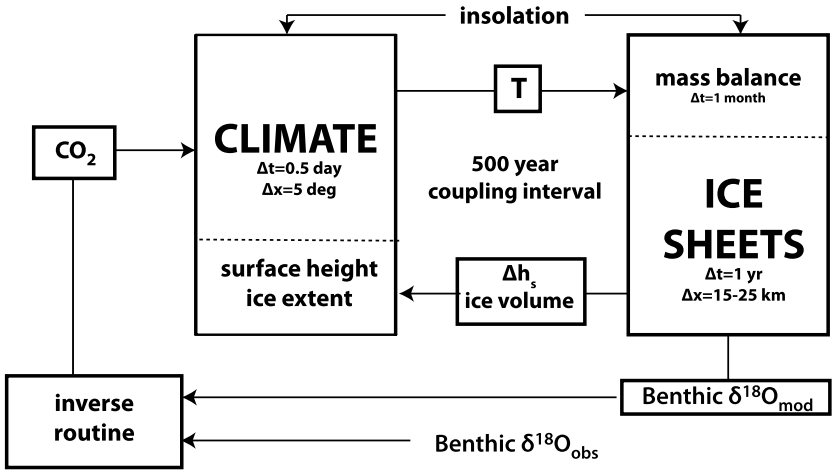

Figure 1. Schematic overview of the coupled model. Information on local temperature (T) is transferred from the climate model to the ice sheet model every 500 model years. The ice sheet model returns surface height and ice volume changes to the climate model. Also, every 500 years, the inverse routine is used to obtain the CO_2 input for the climate model from the difference between modeled benthic $\delta^{18}O$ and an observed $\delta^{18}O$ value 500 years later. For the benthic $\delta^{18}O$ observations the stacked records of *Zachos et al.* [2008, Z08] and *Cramer et al.* [2009, C09] are used. Insolation input [*Laskar et al.*, 2004] is updated every 1000 years.

where T, α, and Q are local temperature, surface albedo, and radiation, incorporating Milankovitch radiation variations, respectively. Parameter C_{abl} determines the ablation threshold. For the East Antarctic ice sheet, it is set to −30 in the reference simulation; in the simulations with increased ablation it is increased to −5. The ice sheet model calculates ice flow using the Shallow Ice Approximation (SIA). The resulting surface height and surface-type changes are forwarded to the climate model, effectuating the surface-height-temperature and albedo-temperature feedbacks. Exchange of variables between the climate and ice sheet models takes place every 500 model years.

The coupled model is forced with insolation data [*Laskar et al.*, 2004], which is updated every 1000 years. In forward mode, forced by CO_2 prescribed by the EPICA Dome C record [*EPICA community members*, 2004], the coupled model is capable of reproducing the glacial-interglacial cycles of the past 800 kyr accurately in terms of temperature and sea level [*Stap et al.*, 2014]. In inverse mode, as used in this study, the CO_2 concentrations are obtained every 500 years from

$$CO_2 = \overline{CO_2} \times \exp\left[c \times \left\{\delta^{18}O(t) - \delta^{18}O_{obs}(t + 0.5\text{kyr})\right\}\right], \quad (3)$$

where $\delta^{18}O(t)$ is the benthic $\delta^{18}O$ calculated by the model as a function of ice temperatures, ice thicknesses, and deep-sea temperature [*De Boer et al.*, 2010] and $\delta^{18}O_{obs}(t + 0.5\text{kyr})$ is the observed $\delta^{18}O$ value 500 years later. Furthermore, $\overline{CO_2}$ is the mean CO_2 concentration of the preceding 15 kyr, and c a strength-determining parameter [*Stap et al.*, 2016]. In earlier work, this inverse routine was shown to reconstruct CO_2 over the past 800 kyr in good agreement with the EPICA Dome C ice core record [*EPICA community members*, 2004; *Stap et al.*, 2016]. Figure 1 shows the coupling between the models, and the forcing, schematically.

In this study, we use the stacked records of *Zachos et al.* [2008, Z08] and *Cramer et al.* [2009, C09] for the observed benthic $\delta^{18}O$ record. These stacked records possess uncertainty due to the fact that they are composed of data records originating from different locations, oceanic settings, and foraminiferal species [*Zachos et al.*, 2008; *Cramer et al.*, 2009]. Nonetheless, we assume them to represent global average conditions. We simulate continuous mutually consistent records of benthic $\delta^{18}O$, CO_2, sea level (ice volume equivalent), and global temperature over the period 38 to 10 Myr ago. In this way, we obtain simulations that transiently cover both the EOT and the MMCO, which are the focus of this study. On the original 1000 year resolution (as used in *Stap et al.* [2016]), the reference run shows larger variability in $\delta^{18}O$ than Z08 (RMSE = 0.42‰). This is because the inverse method yields too much variability in CO_2, leading to oversized fluctuations in $\delta^{18}O$. However, if 40 kyr running averages are considered, the inverse method is very accurate ($r^2 = 0.99$, RMSE = 0.05‰).

Table 1. Description of the Transient Model Runs Over the Period 38 to 10 Myr Ago[a]

Name	Description	Forcing	EAIS C_{abl}	Initial Topo Change (m)	Topo Change Period (Myr Ago)
REF	Reference run	Z08	−30	0	NA
CRAM	Different forcing	C09	−30	0	NA
ABL+	Increased ablation EAIS	Z08	−5	0	NA
TOPO−	Higher Antarctica decreased	Z08	−5	520	34–0
TOPO+	Higher Antarctica increased	Z08	−5	790	34–0
TOPO-Q	Higher Antarctica accelerated	Z08	−5	655	34–20

[a]Forcing records are the stacked benthic δ^{18}O records of *Zachos et al.* [2008, Z08] and *Cramer et al.* [2009, C09]. The ablation threshold parameter (C_{abl}) is defined in equation (2). Topographic changes are applied to the area 60–90°S in the climate model and to the ice sheet models for the East and West Antarctic Ice Sheets (EAIS and WAIS). NA = not applicable.

Therefore, all model input and output data are displayed as 40 kyr running averages in this study, unless otherwise stated. Hence, variations on smaller time scales than 40 kyr can and will not be assessed. Table 1 summarizes all the model runs we performed.

3. Results and Discussion

3.1. The MMCO-EOT Conundrum

Our reference simulation is obtained by running the model over the period 38 to 10 Myr ago, after a spin-up of 2 Myr (Table 1). The stacked benthic δ^{18}O record of *Zachos et al.* [2008, Z08] is used as input. This simulation shows an only partly glaciated Antarctica, sustained by high CO_2 concentrations of 650 to 750 ppm, until the Eocene-Oligocene Transition (EOT; 33.9 Myr ago) (Figure 2). At this time, a CO_2 drop to 325 ppm leads to full-scale glaciation of Antarctica and a 2.6 K global temperature cooling. After this event, the East Antarctic ice sheet remains very variable in size (sea level varying between 0 and 50 m sea level equivalent (s.l.e.) above preindustrial (PI) level) during the Oligocene and early Miocene. This is sustained by CO_2 levels between 400 and 750 ppm, with global mean temperature varying between 289 and 292 K. At the Middle-Miocene Climatic Optimum (MMCO; 17 Myr ago), sea level and CO_2 peak at 55 m above PI and 750 ppm, respectively. Thus, in this simulation the CO_2 concentrations at the MMCO and right before the EOT are similar, meaning there is no sign of hysteresis in the relation between δ^{18}O and CO_2. While this is in agreement with the findings of *Hansen et al.* [2013], who imposed a nonchanging relation between CO_2 and benthic δ^{18}O via temperature, proxy-CO_2 data suggest different CO_2 levels between these two episodes. This is visible in Figure 3 (red line), where we focus on two periods that enclose these warm spells: (a) middle Miocene: 18 to 13 Myr ago and (b) early Oligocene: 35 to 30 Myr ago. We compare our simulated CO_2 to proxy data based on alkenones [*Pagani et al.*, 1999, 2011], boron isotopes [*Foster et al.*, 2012; *Greenop et al.*, 2014; *Pearson et al.*, 2009], and stomata [*Retallack*, 2009; *Kürschner et al.*, 2008]. Before the EOT, there is broad agreement on CO_2 levels ranging from 800 to 1000 ppm between the model results and the data based on alkenones [*Pagani et al.*, 1999] and stomata [*Retallack*, 2009] (Figure 3b). The boron isotope-based reconstruction of *Pearson et al.* [2009] shows slightly higher CO_2 values. Our modeled glaciation threshold CO_2 concentration of approximately 700 ppm is within the 560 to 920 ppm range found by *Gasson et al.* [2014], who studied different combinations of an ice dynamical model coupled to seven climate models (Figure 3b, yellow shading). During the early Oligocene period after the EOT, our reconstructed CO_2 is generally lower than proxy data. The paradoxical simultaneous occurrence of relatively low CO_2 and low δ^{18}O, indicative of high sea level, during the MMCO is very hard to capture. Earlier modeling studies either showed high CO_2 and high sea level [*Langebroek et al.*, 2009, 2010; *Henrot et al.*, 2010; *Goldner et al.*, 2014] or low CO_2 and relatively low sea level [*You et al.*, 2009]. In our reference run, we do not simulate low sea level, because the δ^{18}O in the forcing record [*Zachos et al.*, 2008] is too low. Our simulated sea level is in fact similarly high as before the EOT, implying a similar contribution of sea level and temperature to the δ^{18}O signal. In contrast to our simulation, proxy data show much lower CO_2 concentrations during the MMCO than before the EOT (Figure 3a), although the uncertainties in these reconstructions are substantial. Stomata-based data [*Kürschner et al.*, 2008] ranges between 293 and 469 ppm, while alkenone-based [*Pagani et al.*, 1999] and boron-isotope-based [*Foster et al.*, 2012; *Greenop et al.*, 2014] data show generally lower values of 195 to 540 ppm during the MMCO. The question now arises, what could cause this disagreement between model and data?

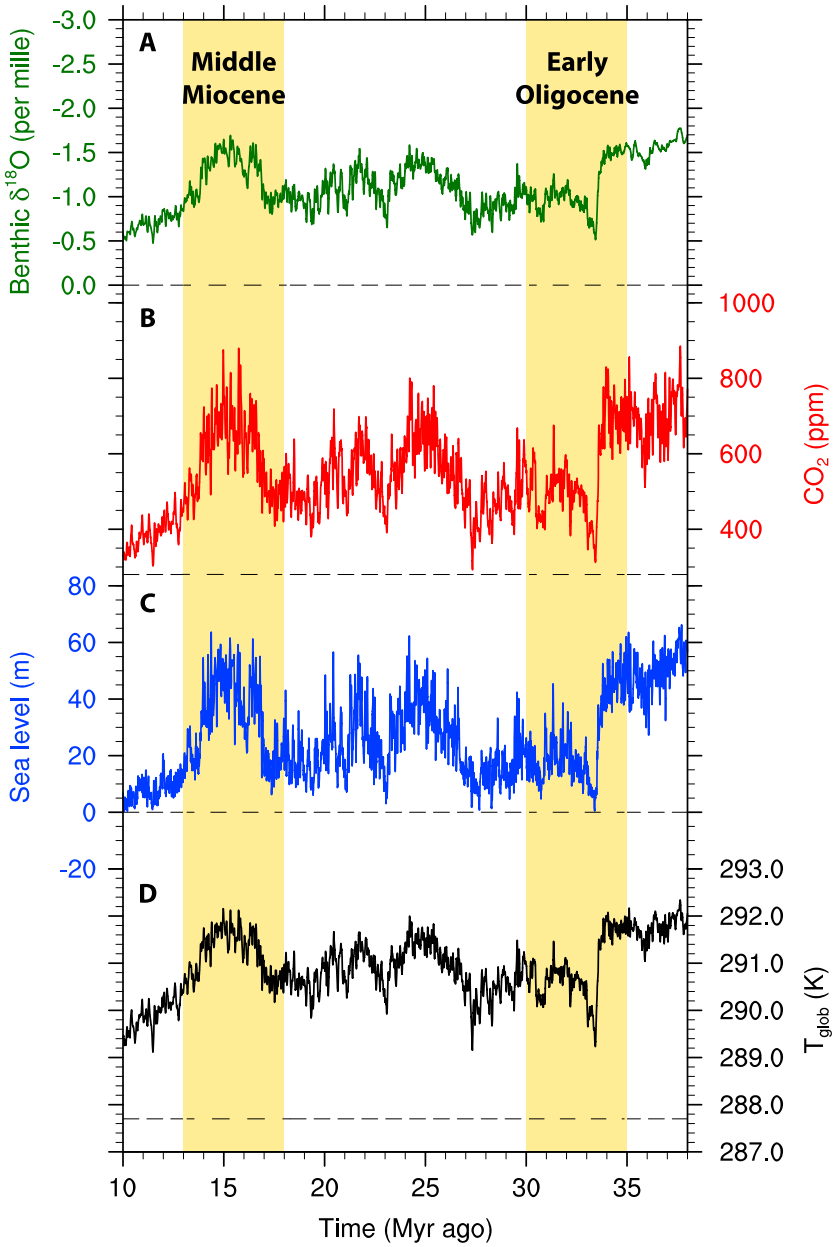

Figure 2. Time series of benthic $\delta^{18}O$, CO_2, sea level, and global temperature. (a) Simulated benthic $\delta^{18}O$, (b) simulated CO_2, (c) simulated sea level in meters above present day, and (d) simulated global mean temperature (T_{glob}). Shown are 40 kyr running averages of the reference run (REF). Dotted lines represent preindustrial (PI) values. Highlighted in yellow are the early Oligocene period (35 to 30 Myr ago) and the middle Miocene period (18 to 13 Myr ago).

Obviously, our reconstruction depends strongly on the $\delta^{18}O$ record that is used as forcing. In another run (CRAM), we force the coupled model with the stacked $\delta^{18}O$ record of *Cramer et al.* [2009, C09] (Table 1). In contrast to Z08, this compilation takes into account differences between ocean basins in the stacking method. The main difference with REF in simulated CO_2 is the timing of full-scale Antarctic glaciation at the EOT and after the MMCO; in simulation CRAM this takes place earlier than in REF. Although the higher $\delta^{18}O$ during the middle to late Miocene in C09 is reflected in lower sea level (not shown), the difference in CO_2 between REF and CRAM is relatively small. This is because the Antarctic Ice Sheet is very sensitive in this CO_2 regime; a small shift in CO_2 leads to a large ice volume change. Hence, both by forcing with C09 and Z08, the simulated difference between CO_2 levels before the EOT and during the MMCO are qualitatively similar.

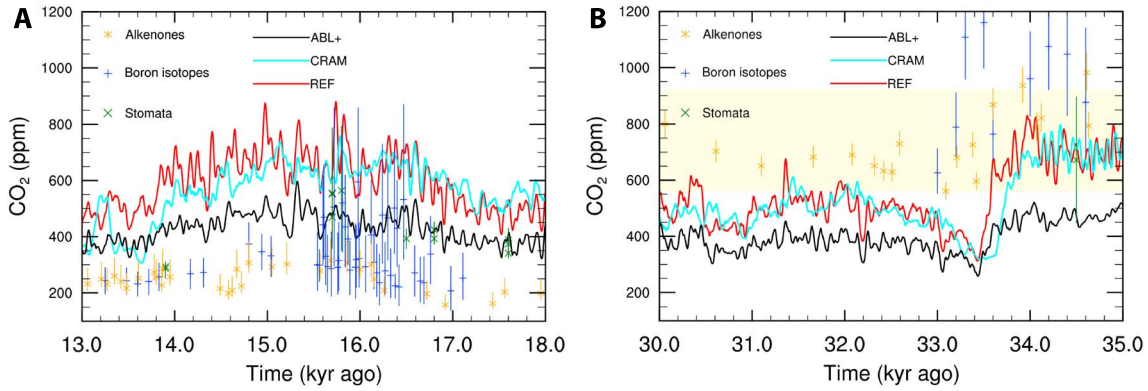

Figure 3. Simulated CO_2 concentrations. Simulated CO_2 for REF (red), CRAM (cyan), and ABL+ (black) for (a) the middle Miocene and (b) the early Oligocene. Symbols indicate proxy-data reconstructions based on alkenones [*Pagani et al.*, 1999, 2011] (orange asterisks), boron isotopes [*Foster et al.*, 2012; *Greenop et al.*, 2014; *Pearson et al.*, 2009] (blue pluses), and stomata data [*Retallack*, 2009; *Kürschner et al.*, 2008] (green crosses). Yellow shading indicates the range of Antarctic glaciation values found by *Gasson et al.* [2014].

An important model uncertainty resides in the mass balance parametrization of the East Antarctic Ice Sheet (EAIS). *Stap et al.* [2016] already showed that increasing the ablation by implementing a lower ablation threshold, leads to a more dynamic EAIS during the Pliocene. We perform a similar experiment (ABL+) forcing the model over the period 38 to 10 Myr ago using Z08 and lowering (in absolute sense) the ablation threshold parameter from its reference value −30 to −5 (Table 1). The increased ablation in this run leads to a decreased threshold CO_2 values for East Antarctic glaciation and deglaciation. Consequently, the resulting CO_2 levels right before the EOT and during the MMCO are lower in the ABL+ simulation than in the REF simulation. This also induces a new balance in the contributions to the benthic $\delta^{18}O$ signal. Since CO_2 is lower, deep-sea temperatures are lower, and hence, ice volume must contribute less to the signal and simulated sea level is somewhat higher (not shown). The simulated lower MMCO CO_2 levels are in better agreement with proxy data (Figure 3a; black line). Contrarily, late Eocene and early Oligocene CO_2 concentrations are now unrealistically low (Figure 3b; black line). In other words, a difference in CO_2 levels between both periods is still not simulated, so the conundrum remains.

The similarity between the early Oligocene and middle Miocene periods in this run is also reflected by the polar amplification in the Southern Hemisphere (Figure 4a). In agreement with data reconstructions [e.g., *Goldner et al.*, 2014; *Bijl et al.*, 2009], we simulate reduced equator-to-South-Pole temperature gradients

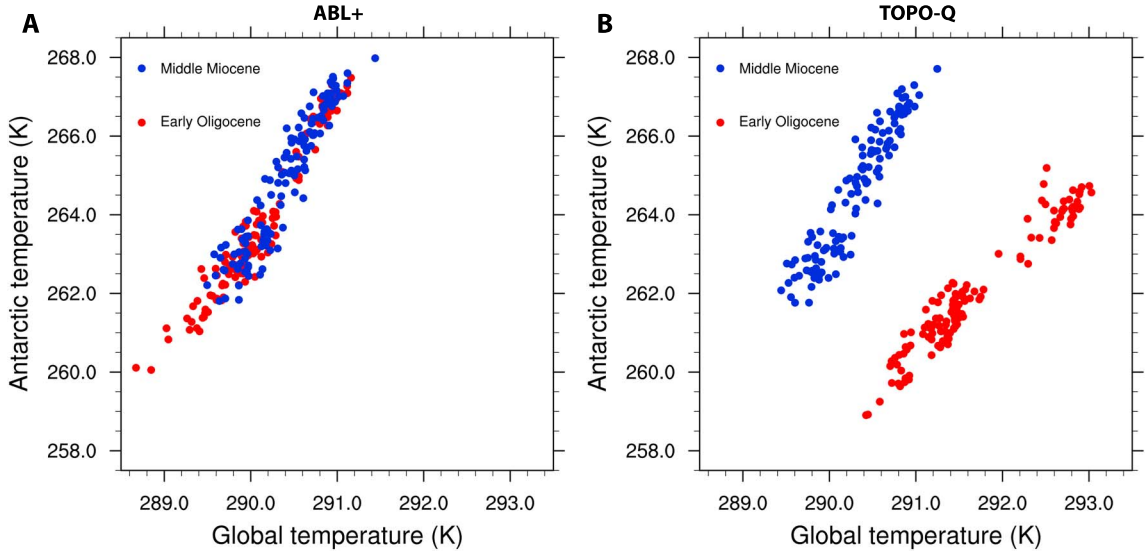

Figure 4. Transient polar amplification. Relation between global and Antarctic (60° to 90°S) mean annual surface temperature, during the middle Miocene (blue dots) and the early Oligocene (red dots). For (a) ABL+ and (b) TOPO-Q.

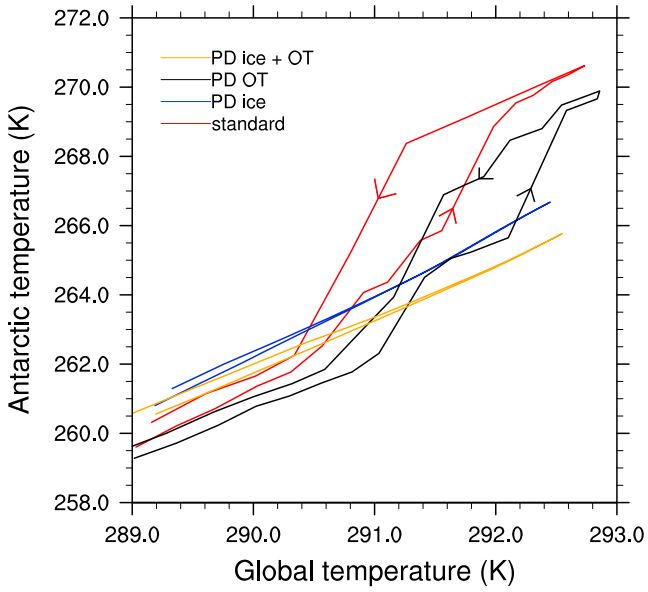

Figure 5. Polar amplification. Relation between global and Antarctic (60 to 90°S) mean annual surface temperature in schematic equilibrium runs using the standard configuration (red), PD land ice conditions (blue), PD ocean overturning strength (black), and PD land ice and ocean overturning strength (orange).

right before the EOT and during the MMCO. This is demonstrated by more strongly increased Antarctic temperatures (up to 9 K) compared to the global mean (up to 3 K) with respect to PD. To investigate the factors determining polar amplification, we additionally perform schematic equilibrium runs of the model. In these runs, we first increase CO_2 in steps of 50 ppm per 50 kyr from 450 ppm to 1200 ppm and then oppositely decrease the concentration back to 450 ppm. Insolation is kept at present-day configuration throughout all these schematic runs. If we do not take into account changing land ice and changing ocean overturning strength, the polar amplification is relatively small and uniform (Figure 5, orange line). Allowing for ocean overturning strength variations increases the amplitude of polar amplification as is indicated in Figure 5 by a slightly steeper blue line. Switching on land ice changes also leads to nonuniform polar amplification (Figure 5, black line). In the latter case, it becomes stronger in the temperature regime where the Antarctic Ice Sheet is dynamic and hence very sensitive to temperature changes. In addition, significant hysteresis is introduced by the surface-height-temperature and albedo-temperature feedbacks, as is shown by the difference between the upward and the downward branches. The separate effects of ocean overturning strength and land ice changes combine more or less linearly (Figure 5, red line).

3.2. Influence of Changing Antarctic Topography

3.2.1. Bulk Effect

In all the runs discussed so far we use present-day topography as boundary condition by assuming a local isostatic equilibrium. However, as a consequence of, e.g., tectonics and erosion, ice-free topography has significantly changed since the late Eocene [*Rugenstein et al.*, 2014, and references therein]. Particularly, the Antarctic topographical changes may have had a significant influence on the dynamics of the Antarctic ice sheet [*Siegert*, 2008; *Oerlemans*, 1984; *Huybrechts*, 1993; *Wilson et al.*, 2013; *Gasson et al.*, 2015; *Austermann et al.*, 2015; *Gasson et al.*, 2016]. *Wilson et al.* [2012] calculated late Eocene Antarctic topography relative to the isostatically rebounded BEDMAP present-day topography [*Lythe et al.*, 2001], using a set of tools including ice sheet-erosion models, models of thermal subsidence, and plate movement. They constructed a minimum and maximum estimated late Eocene topography difference from present day. This study shows eroded volumes that lower the Antarctic continent by 520 to 790 m on average. We perform experiments, where we increase the initial height of the Antarctic continent 38 Myr ago by 520 m (TOPO−) and by 790 m (TOPO+) in the climate model (60 to 90°S) as well as in the ice sheet models of East and West Antarctica. We thereby ignore isostatic adjustment of the eroded material, which counteract lowering of the surface. Our modeling effort therefore probably overestimates the effect of erosion and should be seen as a proof of concept rather than a rigorous quantification. Since not much is known of Antarctic topography evolution over time, we impose a linear decrease of the height difference over time. Data-based evidence suggests that erosion on Antarctica was very weak until glaciation of the continent [*Thomson et al.*, 2013]. Therefore, we start this decrease at 34 Myr ago. The rate of height decrease is such that zero difference would be obtained at present day. However, because Antarctica may have eroded more strongly during the early parts of the Cenozoic [*Tochilin et al.*, 2012], we perform a separate run (TOPO-Q) where the rate of topographic change is quicker. In that run, we prescribe a height decrease of 655 m (the average of 520 and 790 m) linearly over the shorter period 34 to 20 Myr ago. In all these runs, we use the enhanced ablation parameterization of run ABL+ (Table 1), since this gives the best agreement with proxy data during the MMCO.

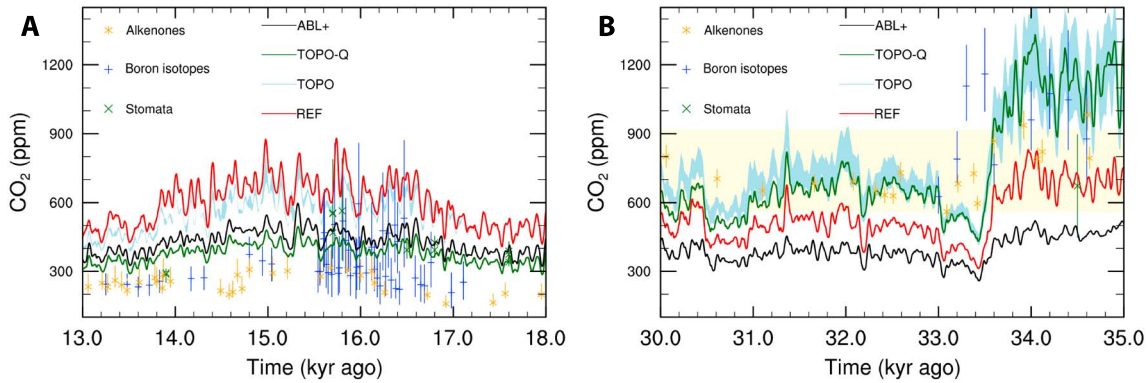

Figure 6. Simulated CO_2 concentrations. Simulated CO_2 for REF (red), TOPO-Q (green), and the range bounded by TOPO− and TOPO+ (blue shading) for (a) the middle Miocene and (b) the early Oligocene. Yellow shading indicates the range of Antarctic glaciation values found by *Gasson et al.* [2014]. Symbols as in Figure 3.

A higher Antarctic surface at the EOT generally experiences lower surface air temperatures at the same CO_2 level. Therefore, the threshold CO_2 value for (de)glaciation is higher. Because the model is forced by the same values of benthic $\delta^{18}O$, in the TOPO experiments we obtain compensating higher levels of CO_2 than in the ABL+ experiment (Figure 6b); even higher than simulated in the REF experiment. The modeled CO_2 ranges from 900 to 1400 ppm before and from 500 to 900 ppm after the EOT, in better agreement with proxy data. At the MMCO, the topographic difference between the TOPO runs and ABL+ has reduced, and simulated CO_2 levels are closer together (Figure 6a). The TOPO− and TOPO+ runs show CO_2 levels almost equal to REF (Figure 6a; blue shading). The CO_2 range spanned by TOPO− and TOPO+ is also smaller because the topographic difference between these runs is reduced. The CO_2 levels simulated in run TOPO-Q are similarly high as ABL+ at the MMCO, since there is no difference in topography with ABL+ at this time anymore (Figure 6a; green line). Any difference in CO_2 is therefore explained by transient effects. Hence, a changing Antarctic surface topography leads to a difference in CO_2 between right before the EOT and during the MMCO, while similar benthic $\delta^{18}O$ is simulated.

A changing relation between Antarctic and global mean temperatures over time is also shown by Figure 4b. During the early Oligocene period, much higher global mean temperatures are simulated by the TOPO-Q simulation than during the middle Miocene period. While similar Antarctic surface temperatures are needed to glaciate the continent, the higher surface elevation ensures that Antarctica is colder with respect to the rest of the globe. Therefore, Antarctica glaciates at higher global mean temperatures, and hence higher concentrations of CO_2. Over the course of time, when the Antarctic surface elevation drops (Figure 7e), the CO_2 levels needed (Figure 7b) to simulate the same benthic $\delta^{18}O$ (Figure 7a) gradually decrease. This concurs with slowly declining global temperatures (Figure 7d). Additionally, simulated sea level before the EOT is lower than during the MMCO (Figure 7c), ~10 m lower than the 40–50 m above present day reconstructed by *Miller et al.* [2005b]. This is because at the EOT, CO_2 levels are increased, leading to warmer deep-sea temperatures. This ensures that a smaller part of the benthic $\delta^{18}O$ decrease with respect to the preindustrial value is accounted for by loss of land ice.

3.2.2. Separate Effect of Several Factors

Having shown the bulk effect of changing Antarctic topography, we recognize that we do not include local effects which may be of importance [*Gasson et al.*, 2015; *Jamieson et al.*, 2010]. The crude resolution of our climate model, as well as the idealized topography of our ice sheet model, hinders doing this. However, in the following we attempt to quantify the uncertainty pertaining to not including local effects by investigating three potentially important factors: (1) the effect of separate EAIS and WAIS height increases (separated E/W in Figure 8), (2) the effect of eliminating the land surface area increase caused by the height increase (decreased area in Figure 8), and (3) the effect of not changing the central height but instead reducing the slope of the EAIS and WAIS (reduced H_{cnt} in Figure 8). To study these effects, we perform three further tests over the shorter period 38 to 30 Myr ago. In these experiments, we do not include any transient changes. Therefore, we also perform a new standard run for comparison, where this time we increase the Antarctic topography by 655 m over the entire run (standard in Figure 8).

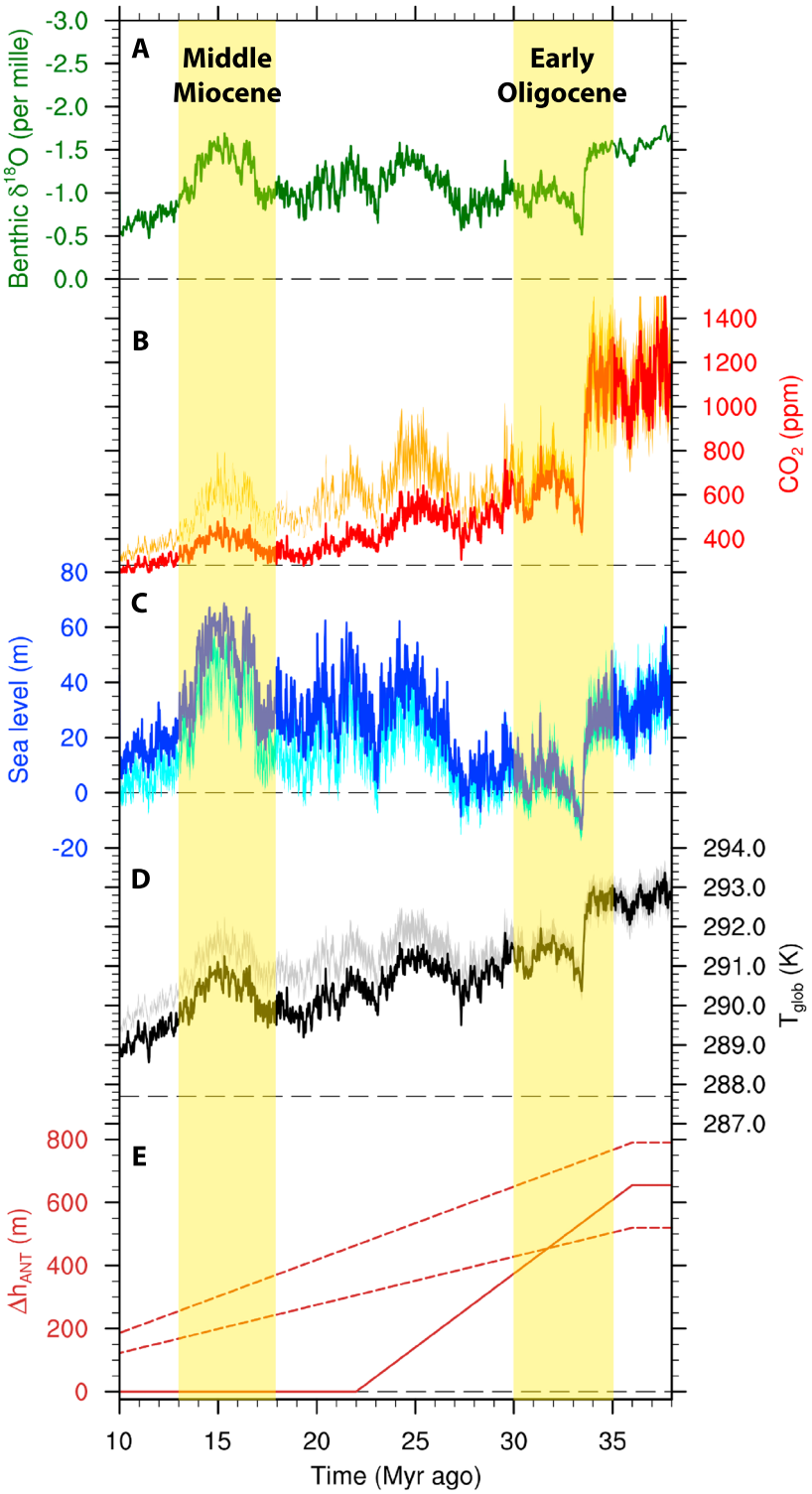

Figure 7. Time series of benthic $\delta^{18}O$, CO_2, Antarctic surface elevation deviation from PD, and global temperature. (a) Simulated benthic $\delta^{18}O$ from TOPO-Q, (b) simulated CO_2 from TOPO-Q (red line) and from TOPO– and TOPO+ (orange shading), (c) simulated sea level in meters above present day from TOPO-Q (blue line) and from TOPO– and TOPO+ (cyan shading), (d) simulated global mean temperature (T_{glob}) from TOPO-Q (black line) and from TOPO– and TOPO+ (grey shading), and (e) Antarctic surface elevation deviation from PD and from TOPO-Q (solid line) and TOPO– and TOPO+ (dashed lines). Shown are 40 kyr running averages. Dotted lines represent preindustrial (PI) values. Highlighted in yellow are the early Oligocene period (35 to 30 Myr ago) and the middle Miocene period (18 to 13 Myr ago).

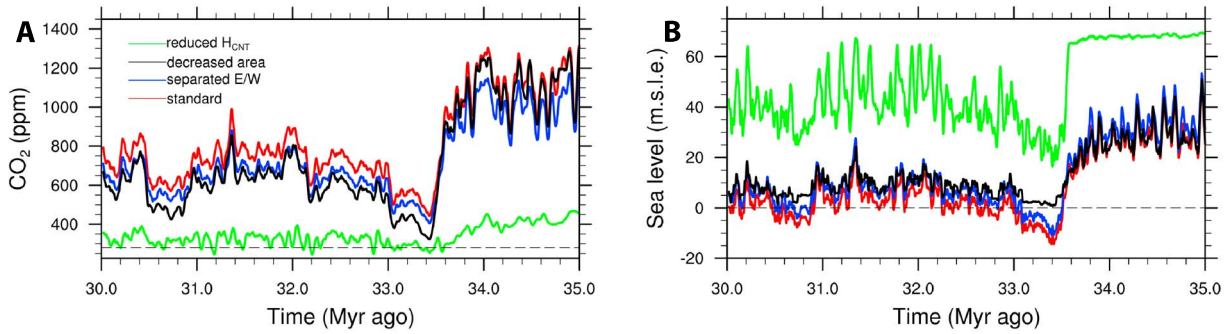

Figure 8. Simulated CO_2 concentrations and sea level. (a) Simulated CO_2 and (b) sea level for the runs performed in section 3.2.2. In red, the standard run with and increased Antarctic height of 655 m. In blue, the run with separate height increases of 401 m for the EAIS and 865 m for the WAIS. In black, the run with increased height of 655 m, but reduced surface area. In green, the run without central height (H_{CNT}) increase, but with a reduced slopes for the EAIS and WAIS.

In the first test, we make a distinction between the topography of the EAIS and the WAIS, as evidence suggests that the WAIS eroded more than the EAIS. We apply a height increase of 401 m to the EAIS, and 865 m to the WAIS. This is based on separating the eroded volumes of both these areas in Table 3 of *Wilson et al.* [2012]. Doing this slightly hinders the growth of land ice, leading to 101 ppm lower CO_2 concentrations (Figure 8a, blue line), and 4.8 m higher sea level (Figure 8b, blue line) averaged over the whole simulated period 38 to 30 Myr ago.

The 655 m height increase we apply facilitates the Antarctic surface area above sea level becoming 243% larger when there is no land ice (a contribution of 70 m sea level), and 235% larger at present-day sea level. This leads to an easier build up of more land ice. To quantify this effect, we perform a second test where we artificially eliminate this surface area increase. In addition to applying the 655 m height increase of the topography, we raise the sea level by the same amount. In this way, the Antarctic continent still experiences lower temperatures but does not have a larger land surface area. At high sea levels, there is not much difference with the new standard run (Figure 8, black lines). However, toward colder conditions, land ice growth is capped at approximately present-day sea level. In the new standard run, the Antarctic Ice Sheet grows larger, and sea level drops to −14.4 m at the end of the EOT. This indicates an Antarctic Ice Sheet size of 84.4 m s.l.e., ∼20% larger than present day, in agreement with the 83.4 to 89.5 m s.l.e. range found by *Wilson et al.* [2013]. A smaller Antarctic Ice Sheet leads to a reduced benthic $\delta^{18}O$ signal. This is compensated by lower deep-sea temperatures, and hence decreased CO_2. After the EOT CO_2 is on average 105 ppm and maximally 159 ppm lower than in the new standard run.

Finally, in our model the glacial inception threshold may be contingent on the height of the top of the continental cone, where glaciation starts. Translated to the real world, this implies a dependency on the height of the mountainous regions of the Antarctic continent. These regions, however, may not have eroded as much as the lower lying parts of Antarctica [*Rose et al.*, 2013]. Therefore, in the third test we do not increase the central height of the continents but reduce the slopes such that the volume above sea level remains the same as in the new standard run. This means a slope of −0.474 instead of −1.0 m/km for the EAIS, and a slope of −0.158 instead of −1.1 m/km for the WAIS. Clearly, this has a very large effect on the simulated CO_2 (Figure 8a, green line) and sea level (Figure 8b, green line). In this simulation CO_2 and sea level are hardly different from the ABL+ results (not shown), being, respectively, much lower and higher than in the new standard run.

3.3. Other Influencing Factors

Other important factors that can affect the glaciation threshold CO_2 are ocean dynamics and vegetation dynamics. In our model, we use a simple meridional overturning scheme for the ocean [*Bintanja*, 1997; *Stap et al.*, 2014]. The strength of the overturning is determined by the density difference between equatorial and polar waters. In reality, however, a change in the structure of the ocean basins can also have a significant effect on ocean dynamics. For instance, closure of the Drake Passage has a lowering effect on the Antarctic glaciation CO_2 threshold at the EOT [*Kenneth*, 1977; *DeConto and Pollard*, 2003; *Toggweiler and Bjornsson*, 2000] by increasing ocean heat transport toward the South Pole. Another data study argued that a deeper global thermocline and reduced low-latitude gradients in sea surface temperature during the Miocene may explain an altered relation between CO_2 and temperature [*LaRiviere et al.*, 2012]. Furthermore, we ignore vegetation dynamics. In our model, the Antarctic continent is covered by grassland when it is ice free. If the vegetation

consisted (partly) of forests during the EOT, the CO_2 threshold for Antarctic glaciation could be much lower [*Liakka et al.*, 2014]. These mechanisms would favor higher CO_2 at the MMCO than at the EOT opposite to what the data suggest. Therefore, we leave analysis of the impact of these factors to studies using more sophisticated models that contain more detailed ocean and vegetation physics.

4. Conclusions

We have presented continuous mutually consistent simulations of benthic $\delta^{18}O$, CO_2, sea level, and global temperature, over the period 38 to 10 Myr ago (Figure 2). These are obtained using a coupled climate-ice sheet model, with an inverse routine to get CO_2 from a stacked benthic $\delta^{18}O$ record [*Zachos et al.*, 2008; *Cramer et al.*, 2009]. This approach based on simplified models provides the unique possibility of reconciling these variables on multimillion year time scales.

We have focused on two warm spells, the EOT and the MMCO, where proxy data suggest different CO_2 levels, while benthic $\delta^{18}O$ values are similar. We find that this conundrum cannot be explained using the standard configuration of our model. We simulate similar CO_2 levels right before the EOT as during the MMCO. The contributions of ice volume and deep-sea temperature to the benthic $\delta^{18}O$ signal during these two episodes are also comparable. Forcing the model by the benthic $\delta^{18}O$ record of *Cramer et al.* [2009], which shows higher values during the middle Miocene, we do obtain lower sea level. The simulated CO_2 levels, however, are only slightly reduced. Lowering the uncertain ablation threshold for the EAIS leads to decreasing levels of CO_2 at both events and therefore offers no solution to the conundrum.

In order to offer a solution to the conundrum, we investigate the first-order effect of evolving Antarctic topography. For this purpose, we run the model starting with a height increase of 520 to 790 m based on the eroded volumes in *Wilson et al.* [2012] applied to the Antarctic continent. We diminish this height increase either slowly (to reach zero at present day) or more quickly (to reach zero at 20 Myr ago). Through the lapse rate effect, a higher surface at the EOT experiences lower temperatures. This means that the EAIS glaciates and deglaciates at higher CO_2 levels. Therefore, low benthic $\delta^{18}O$ values are reached at these increased CO_2 levels and contain a comparatively larger contribution from warmer deep-sea temperatures. Especially when the topographic difference is reduced at a relatively fast pace, this offers an explanation for differences in CO_2 between the EOT and MMCO while benthic $\delta^{18}O$ values are similar. Additionally, the larger land mass effectuated by the height increase can sustain a 20% larger Antarctic ice sheet. When spatial heterogeneity is included by applying different height increases for the EAIS and WAIS separately, the CO_2 difference is somewhat (~100 ppm) reduced.

The effect of increased Antarctic surface elevation is, however, strongly contingent on how the 3-D topographic changes are implemented in the 1-D ice sheet model. The threshold for (de)glaciation in our model is determined by the maximum height of the continental cone. If instead of applying a uniform height increase, this peak height is kept constant and only the slope of the Antarctic continent is reduced, the simulated EOT CO_2 is much lower. Therefore, to better constrain the influence of erosion and tectonic movement on climate, a 3-D ice sheet model should be used. Ideally, this model would be interactively coupled to an erosion model. Inclusion of isostatic adjustment should further help to obtain more realistic results.

Acknowledgments
The results presented in this paper are available online at doi:10.5281/zenodo.56676. We thank two anonymous referees, who have given constructive and clear comments that have helped to improve the paper substantially. Furthermore, we thank Stewart Jamieson for providing information on the reconstruction of Antarctic topography. Financial support for L.B. Stap was provided by the Netherlands Organisation of Scientific Research NWO-ALW grant. B. de Boer receives funding from the European Union's Horizon 2020 research and innovation program under the Marie Sklodowska-Curie grant agreement 660814.

References

Austermann, J., D. Pollard, J. X. Mitrovica, R. Moucha, A. M. Forte, R. M. DeConto, D. B. Rowley, and M. E. Raymo (2015), The impact of dynamic topography change on Antarctic ice sheet stability during the mid-Pliocene warm period, *Geology*, *43*(10), 927–930.

Beerling, D. J., and D. L. Royer (2011), Convergent Cenozoic CO_2 history, *Nat. Geosci.*, *4*(7), 418–420.

Bijl, P. K., S. Schouten, A. Sluijs, G.-J. Reichart, J. C. Zachos, and H. Brinkhuis (2009), Early palaeogene temperature evolution of the Southwest Pacific Ocean, *Nature*, *461*(7265), 776–779.

Bintanja, R. (1997), Sensitivity experiments performed with an energy balance atmosphere model coupled to an advection-diffusion ocean model, *Theor. Appl. Climatol.*, *56*(1–2), 1–24.

Bintanja, R., and R. S. W. Van de Wal (2008), North American ice-sheet dynamics and the onset of 100,000-year glacial cycles, *Nature*, *454*(7206), 869–872.

Bintanja, R., R. S. W. van de Wal, and J. Oerlemans (2005), Modelled atmospheric temperatures and global sea levels over the past million years, *Nature*, *437*(7055), 125–128.

Chappell, J., and N. Shackleton (1986), Oxygen isotopes and sea level, *Nature*, *324*(6093), 137–140.

Cramer, B., J. Toggweiler, J. Wright, M. Katz, and K. Miller (2009), Ocean overturning since the Late Cretaceous: Inferences from a new benthic foraminiferal isotope compilation, *Paleoceanography*, *24*, PA4216, doi:10.1029/2008PA001683.

De Boer, B., R. S. W. Van de Wal, R. Bintanja, L. J. Lourens, and E. Tuenter (2010), Cenozoic global ice-volume and temperature simulations with 1-D ice-sheet models forced by benthic $\delta^{18}O$ records, *Ann. Glaciol.*, *51*(55), 23–33.

De Boer, B., R. S. W. Van de Wal, L. J. Lourens, R. Bintanja, and T. Reerink (2013), A continuous simulation of global ice volume over the past 1 million years with 3-D ice-sheet models, *Clim. Dyn.*, *41*(5–6), 1365–1384.
De Boer, B., L. J. Lourens, and R. S. W. van de Wal (2014), Persistent 400,000-year variability of Antarctic ice volume and the carbon cycle is revealed throughout the Plio-Pleistocene, *Nat. Commun.*, *5*, 2999, doi:10.1038/ncomms3999.
DeConto, R. M., and D. Pollard (2003), Rapid Cenozoic glaciation of Antarctica induced by declining atmospheric CO_2, *Nature*, *421*(6920), 245–249.
Elderfield, H., P. Ferretti, M. Greaves, S. Crowhurst, I. McCave, D. Hodell, and A. Piotrowski (2012), Evolution of ocean temperature and ice volume through the Mid-Pleistocene climate transition, *Science*, *337*(6095), 704–709.
EPICA community members (2004), Eight glacial cycles from an Antarctic ice core, *Nature*, *429*(6992), 623–628.
EPICA community members (2006), One-to-one coupling of glacial climate variability in Greenland and Antarctica, *Nature*, *444*(7116), 195–198.
Foster, G. L., and E. J. Rohling (2013), Relationship between sea level and climate forcing by CO_2 on geological timescales, *Proc. Natl. Acad. Sci. U. S. A.*, *110*(4), 1209–1214.
Foster, G. L., C. H. Lear, and J. W. Rae (2012), The evolution of pCO_2, ice volume and climate during the Middle Miocene, *Earth Planet. Sci. Lett.*, *341*, 243–254.
Gasson, E., M. Siddall, D. J. Lunt, O. J. Rackham, C. H. Lear, and D. Pollard (2012), Exploring uncertainties in the relationship between temperature, ice volume, and sea level over the past 50 million years, *Rev. Geophys.*, *50*, RG1005, doi:10.1029/2011RG000358.
Gasson, E., et al. (2014), Uncertainties in the modelled CO_2 threshold for Antarctic glaciation, *Clim. Past*, *10*(2), 451–466.
Gasson, E., R. M. DeConto, and D. Pollard (2015), Antarctic bedrock topography uncertainty and ice sheet stability, *Geophys. Res. Lett.*, *42*, 5372–5377, doi:10.1002/2015GL064322.
Gasson, E., R. M. DeConto, D. Pollard, and R. H. Levy (2016), Dynamic Antarctic ice sheet during the early to mid-Miocene, *Proc. Natl. Acad. Sci. U.S.A.*, *113*(13), 3459–3464.
Goldner, A., N. Herold, and M. Huber (2014), The challenge of simulating the warmth of the Mid-Miocene Climatic Optimum in CESM1, *Clim. Past*, *10*(2), 523–536.
Greenop, R., G. L. Foster, P. A. Wilson, and C. H. Lear (2014), Middle Miocene climate instability associated with high-amplitude CO_2 variability, *Paleoceanography*, *29*, 845–853, doi:10.1002/2014PA002653.
Hansen, J., M. Sato, G. Russell, and P. Kharecha (2013), Climate sensitivity, sea level and atmospheric carbon dioxide, *Philos. Trans. R. Soc. A*, *371*, 20120294.
Henrot, A.-J., L. François, E. Favre, M. Butzin, M. Ouberdous, and G. Munhoven (2010), Effects of CO_2, continental distribution, topography and vegetation changes on the climate at the Middle Miocene: A model study, *Climate of the Past*, *6*(5), 675–694.
Huybrechts, P. (1993), Glaciological modelling of the Late Cenozoic East Antarctic ice sheet: Stability or dynamism?, *Geogr. Ann., Ser. A*, *75*, 221–238.
Imbrie, J., et al. (1992), On the structure and origin of major glaciation cycles: 1. Linear responses to Milankovitch forcing, *Paleoceanography*, *7*(6), 701–738, doi:10.1029/92PA02253.
Jamieson, S. S., D. E. Sugden, and N. R. Hulton (2010), The evolution of the subglacial landscape of Antarctica, *Earth Planet. Sci. Lett.*, *293*(1), 1–27.
Kenneth, J. (1977), Cenozoic evolution of Antarctic glaciation, the circum-Antarctic oceans and their impact on global paleoceanography, *J. Geophys. Res.*, *82*(27), 3843–3859.
Köhler, P., B. de Boer, A. S. von der Heydt, L. B. Stap, and R. S. W. van de Wal (2015), On the state-dependency of the equilibrium climate sensitivity during the last 5 million years, *Clim. Past*, *11*(12), 1801–1823, doi:10.5194/cp-11-1801-2015.
Kominz, M., J. Browning, K. Miller, P. Sugarman, S. Mizintseva, and C. Scotese (2008), Late Cretaceous to Miocene sea-level estimates from the New Jersey and Delaware coastal plain coreholes: An error analysis, *Basin Res.*, *20*(2), 211–226.
Kürschner, W. M., Z. Kvaček, and D. L. Dilcher (2008), The impact of Miocene atmospheric carbon dioxide fluctuations on climate and the evolution of terrestrial ecosystems, *Proc. Natl. Acad. Sci. U. S. A.*, *105*(2), 449–453.
Ladant, J.-B., Y. Donnadieu, and C. Dumas (2014), Links between CO_2, glaciation and water flow: Reconciling the Cenozoic history of the Antarctic circumpolar current, *Clim. Past*, *10*(6), 1957–1966.
Langebroek, P., A. Paul, and M. Schulz (2009), Antarctic ice-sheet response to atmospheric CO_2 and insolation in the Middle Miocene, *Clim. Past*, *5*(4), 633–646.
Langebroek, P., A. Paul, and M. Schulz (2010), Simulating the sea level imprint on marine oxygen isotope records during the Middle Miocene using an ice sheet-climate model, *Paleoceanography*, *25*, PA4203, doi:10.1029/2008PA001704.
LaRiviere, J. P., A. C. Ravelo, A. Crimmins, P. S. Dekens, H. L. Ford, M. Lyle, and M. W. Wara (2012), Late Miocene decoupling of oceanic warmth and atmospheric carbon dioxide forcing, *Nature*, *486*(7401), 97–100.
Laskar, J., P. Robutel, F. Joutel, M. Gastineau, A. Correia, and B. Levrard (2004), A long-term numerical solution for the insolation quantities of the Earth, *Astron. Astrophys.*, *428*(1), 261–285.
Lear, C. H., H. Elderfield, and P. Wilson (2000), Cenozoic deep-sea temperatures and global ice volumes from Mg/Ca in benthic foraminiferal calcite, *Science*, *287*(5451), 269–272.
Liakka, J., F. Colleoni, B. Ahrens, and T. Hickler (2014), The impact of climate-vegetation interactions on the onset of the Antarctic ice sheet, *Geophys. Res. Lett.*, *41*, 1269–1276, doi:10.1002/2013GL058994.
Lisiecki, L. E., and M. E. Raymo (2005), A Pliocene-Pleistocene stack of 57 globally distributed benthic $\delta^{18}O$ records, *Paleoceanography*, *20*, PA1003, doi:10.1029/2004PA001071.
Lythe, M. B., D. J. Vaughan, and the BEDMAP Consortium (2001), BEDMAP: A new ice thickness and subglacial topographic model of Antarctica, *J. Geophys. Res.*, *106*(B6), 11,335–11,351.
Milankovitch, M. (1930), *Mathematische Klimalehre und Astronomische Theorie der Klimaschwankungen*, Gebruder Borntreger, Berlin.
Miller, K. G., M. A. Kominz, J. V. Browning, J. D. Wright, G. S. Mountain, M. E. Katz, P. J. Sugarman, B. S. Cramer, N. Christie-Blick, and S. F. Pekar (2005a), The Phanerozoic record of global sea-level change, *Science*, *310*(5752), 1293–1298.
Miller, K. G., J. D. Wright, and J. V. Browning (2005b), Visions of ice sheets in a greenhouse world, *Mar. Geol.*, *217*, 215–231.
North, G. R. (1975), Theory of energy-balance climate models, *J. Atmos. Sci.*, *32*(11), 2033–2043.
Oerlemans, J. (1984), Numerical experiments on glacial erosion, *Z. Gletscherkd. Glazialgeol.*, *20*, 107–126.
Pagani, M., M. A. Arthur, and K. H. Freeman (1999), Miocene evolution of atmospheric carbon dioxide, *Paleoceanography*, *14*(3), 273–292, doi:10.1029/1999PA900006.
Pagani, M., M. Huber, Z. Liu, S. M. Bohaty, J. Henderiks, W. Sijp, S. Krishnan, and R. M. DeConto (2011), The role of carbon dioxide during the onset of Antarctic glaciation, *Science*, *334*(6060), 1261–1264.

Pearson, P. N., G. L. Foster, and B. S. Wade (2009), Atmospheric carbon dioxide through the Eocene-Oligocene climate transition, *Nature*, *461*(7267), 1110–1113.
Pollard, D., and R. M. DeConto (2005), Hysteresis in Cenozoic Antarctic ice-sheet variations, *Global Planet. Change*, *45*(1), 9–21.
Retallack, G. J. (2009), Greenhouse crises of the past 300 million years, *Geol. Soc. Am. Bull.*, *121*(9–10), 1441–1455.
Rohling, E., G. Foster, K. Grant, G. Marino, A. Roberts, M. Tamisiea, and F. Williams (2014), Sea-level and deep-sea-temperature variability over the past 5.3 million years, *Nature*, *508*(7497), 477–482.
Rose, K. C., F. Ferraccioli, S. S. R. Jamieson, R. E. Bell, H. Corr, T. T. Creyts, D. Braaten, T. A. Jordan, P. T. Fretwell, and D. Damaske (2013), Early East Antarctic Ice Sheet growth recorded in the landscape of the Gamburtsev Subglacial Mountains, *Earth Planet. Sci. Lett.*, *375*, 1–12.
Rugenstein, M., P. Stocchi, A. von der Heydt, H. Dijkstra, and H. Brinkhuis (2014), Emplacement of Antarctic ice sheet mass affects circumpolar ocean flow, *Global Planet. Change*, *118*, 16–24.
Siegert, M. J. (2008), Antarctic subglacial topography and ice-sheet evolution, *Earth Surf. Processes Landforms*, *33*(4), 646–660.
Sosdian, S., and Y. Rosenthal (2009), Deep-sea temperature and ice volume changes across the Pliocene-Pleistocene climate transitions, *Science*, *325*(5938), 306–310.
Stap, L. B., R. S. W. van de Wal, B. de Boer, R. Bintanja, and L. J. Lourens (2014), Interaction of ice sheets and climate during the past 800 000 years, *Clim. Past*, *10*(6), 2135–2152.
Stap, L. B., B. de Boer, M. Ziegler, R. Bintanja, L. J. Lourens, and R. S. W. van de Wal (2016), CO_2 over the past 5 million years: Continuous simulation and new δ^{11}B-based proxy data, *Earth Planet. Sci. Lett.*, *439*, 1–10.
Thomson, S. N., P. W. Reiners, S. R. Hemming, and G. E. Gehrels (2013), The contribution of glacial erosion to shaping the hidden landscape of East Antarctica, *Nat. Geosci.*, *6*(3), 203–207.
Tochilin, C. J., P. W. Reiners, S. N. Thomson, G. E. Gehrels, S. R. Hemming, and E. L. Pierce (2012), Erosional history of the Prydz Bay sector of East Antarctica from detrital apatite and zircon geo-and thermochronology multidating, *Geochem. Geophys. Geosyst.*, *13*, Q11015, doi:10.1029/2012GC004364.
Toggweiler, J., and H. Bjornsson (2000), Drake Passage and palaeoclimate, *J. Quat. Sci.*, *15*(4), 319–328.
Van de Wal, R. S. W., B. de Boer, L. J. Lourens, P. Köhler, and R. Bintanja (2011), Reconstruction of a continuous high-resolution CO_2 record over the past 20 million years, *Clim. Past*, *7*(4), 1459–1469, doi:10.5194/cp-7-1459-2011.
Van den Berg, J., R. S. . W. v. d. Wal, and J. Oerlemans (2008), A mass balance model for the Eurasian ice sheet for the last 120,000 years, *Global Planet. Change*, *61*(3), 194–208.
Wilson, D. S., S. S. Jamieson, P. J. Barrett, G. Leitchenkov, K. Gohl, and R. D. Larter (2012), Antarctic topography at the Eocene-Oligocene boundary, *Palaeogeogr. Palaeoclimatol. Palaeoecol.*, *335*, 24–34.
Wilson, D. S., D. Pollard, R. M. DeConto, S. S. Jamieson, and B. P. Luyendyk (2013), Initiation of the West Antarctic ice sheet and estimates of total Antarctic ice volume in the earliest Oligocene, *Geophys. Res. Lett.*, *40*, 4305–4309, doi:10.1002/grl.50797.
You, Y., M. Huber, R. Müller, C. Poulsen, and J. Ribbe (2009), Simulation of the Middle Miocene climate optimum, *Geophys. Res. Lett.*, *36*, L04702, doi:10.1029/2008GL036571.
Zachos, J. C., G. R. Dickens, and R. E. Zeebe (2008), An early Cenozoic perspective on greenhouse warming and carbon-cycle dynamics, *Nature*, *451*(7176), 279–283.